Analytical Methods

Accepted Manuscript

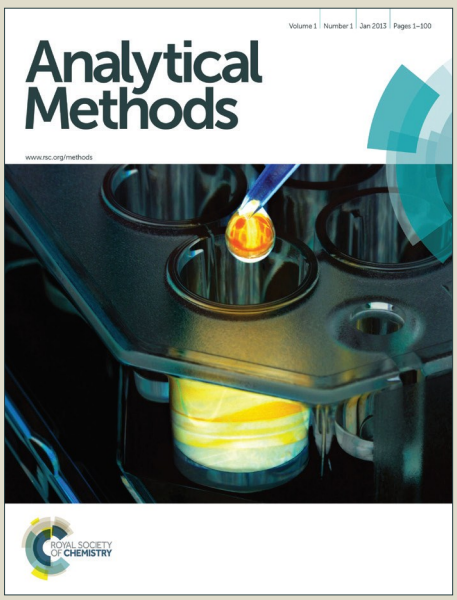

This is an *Accepted Manuscript*, which has been through the Royal Society of Chemistry peer review process and has been accepted for publication.

Accepted Manuscripts are published online shortly after acceptance, before technical editing, formatting and proof reading. Using this free service, authors can make their results available to the community, in citable form, before we publish the edited article. We will replace this *Accepted Manuscript* with the edited and formatted *Advance Article* as soon as it is available.

You can find more information about *Accepted Manuscripts* in the Information for Authors.

Please note that technical editing may introduce minor changes to the text and/or graphics, which may alter content. The journal's standard Terms & Conditions and the Ethical guidelines still apply. In no event shall the Royal Society of Chemistry be held responsible for any errors or omissions in this *Accepted Manuscript* or any consequences arising from the use of any information it contains.

ROYAL SOCIETY OF CHEMISTRY

www.rsc.org/methods

Analytical Methods *19 November* 2015

Nanoporous anodic aluminum oxide films for UV/Vis detection of noble and non-noble metals

Yuliya E. Silina,[1]* Tatiana A. Kychmenko,[2] Marcus Koch[1]

[1]*INM-Leibniz Institute for New Materials, Campus D2 2, 66123 Saarbrücken, Germany*
[2]*Voronezh State University of Engineering Technologies, Voronezh, Russia*

*Corresponding author:

Dr. Yuliya Silina
Chemical Analytics,
INM-Leibniz Institute for New Materials,
Campus D2 2, 66123 Saarbrücken, Germany
Tel: +49 681 9300-117
Fax: +49 681 9300-242
E-Mail: *yuliya.silina@leibniz-inm.de*

Abstract

In this study, a simple, rapid and inexpensive approach for screening with photometric reagents of heavy metals was developed based on porous, anodic aluminium oxide (AAO) films, with detection limits of 0.45 mg/L (Co^{2+}), 0.25 mg/L (Pb^{2+}) and 0.59 mg/L (Ni^{2+}). Noble metal ions Ag^{+} and Pd^{2+}, as well as Cu^{2+}, formed nanoparticles within the AAO channels during micro-solid phase extraction driven by galvanic electroless displacement followed by UV detection.

Keywords: anodic aluminium oxide (AAO), noble/non-noble metals, photometric reagents, UV/Vis detection, nanoparticles.

Introduction

Industrial galvanic production often results in severe environmental pollution by heavy metals [1]. Moreover, the environmental protection laws of many countries do not regulate the maximum concentrations of metal nanoparticles (NPs) in matrices such as waste water in the vicinity of galvanic manufacturing plants [2-5].

Routine analytical procedures for monitoring heavy metals are often based on inductively-coupled plasma optical emission spectroscopy (ICP-OES) [6], which are strongly influenced by matrix interferences and usually require elaborate sample preparation routines for environmental samples [2,6]. Solid-phase spectrophotometry techniques are often less affected by interferences, as they perform metal sorption and direct spectrophotometric detection of the trapped analytes from the same material [7-12]. The solid materials applied for sorption are, for example, gelatine gels, polyacrylamide fibres and carbon nanotubes [8-12]. Their utility in the direct spectrophotometric measurement is often restricted by the limited sorption capacity for metals, however, which then requires very sensitive instrumental detection techniques, *e.g.* X-ray fluorescence or ultraviolet spectroscopy [7]. Furthermore, for rapid detection of heavy metals in environmental samples, whole-cell biosensors based on metallothionein promoters as well as DNA sensors using metal-mediated DNA duplexes have been proposed [13-19]. Unfortunately, the required homogeneity of the reactions and the elaborate detection equipment make them unsuitable for rapid on-site, *in situ* analysis.

In this study, we have developed a simple and rapid method for screening heavy metals from water samples by solid phase micro-extraction of metals with subsequent visual detection. We propose the use of anodic aluminium oxide (AAO) nanoporous films for this purpose. AAO can be readily formed by anodic oxidation of aluminium, resulting highly porous materials with adjustable structures. AAO has been utilized in many applications, including molecular separations, catalysis, energy generation/storage, electronics and photonics, sensors, hybrid nanomaterials and templates, drug delivery and template syntheses [20-26]. AAO exhibits both active acidic and basic centres on the surface, making non-covalent attachment of analytes readily possible through donor-acceptor interactions and hydrogen bonding to the AAO surface *via* appropriate anchor groups [26]. As well, AAO matrices have been successfully utilized as templates for biosensors [28-30] and as substrate material for analysis of peptides by surface assisted laser desorption/ionisation mass spectrometry (SALDI-MS) [31].

Furthermore, metals such as Au, Ag, Cu and *etc.* are readily deposited within pores of AAO substrates by electrochemical deposition on anodic aluminium oxide templates with high efficiency, to obtain protective and decorative coatings [32-34]. No particular attention has been paid so far to the use of both electrochemical and chemical deposition of metals on anodic aluminium oxide surfaces as a means of analytical sampling and detection.We have investigated the analysis of metal ions with different reduction potentials (E^0); *viz.*, Ag^+, Pd^{2+}, Cu^{2+}, Co^{2+}, Ni^{2+} and Pb^{2+}. The approach allowed screening of non-noble metals (Ni^{2+}, Co^{2+}, Pb^{2+}) with photometric reagents and UV-detection of noble Ag^+, Pd^{2+} and Cu^{2+} due to their chemical reduction to nanoparticles in the solid AAO matrix.

Experimental

Chemicals and materials

$CoSO_4$, $Pb(NO_3)_2$, $NiSO_4$, $CuSO_4$, H_2PdO_2, $AgNO_3$, 1-nitroso-2-naphthol-3,6-disulfonic acid disodium salt (nitroso-R-salt, NRS), dithizone, murexide, alizarin red, KI, dimethylglyoxime, sulfosalicylic acid were purchased from Merck (Darmstadt, Germany), 60 μm Al foil (nominal composition of Al98Mg2%) and platinum plate (99.99%) from VWR (Darmstadt, Germany), granular Al_2O_3 (TU 2163-011-51444844-2005, grain size 2-4 mm, pore diameter 0.2-0.5 μm) from AM3 Ltd. (Chelyabinsk, Russia), isopropanol, HCl, acetone, ethanol from Sigma-Aldrich (Steinheim, Germany). Organic-free, deionized water was generated by an Elga PureLab (Celle, Germany) water purification system.

Preparation of AAO matrix

The properties of the synthesized AAO films such as morphology, fragility, inherent colour, porosity, prepared from aluminium foil, strongly depend on the nature of the electrolyte solution as well as parameters such as electrolysis time (t_{el}) and current (I_a). For the preparation of anodic films, a two-step procedure was applied using oxidation of aluminium foil in 0.6 M sulfosalycilic acid as it was optimized in our previous study involved analytical application of AAO [26]. Al foil was initially polished using a series of abrasive papers (9 → 6 → 3 μm). To remove the native layer, an anodic current density of I_a =1 A/dm^2 for $t_{el(1)}$=10 min (first oxidation) was initially applied; during the second oxidation step, the current density ranged from I_a =0.5 to 1.5 A/dm^2 for $t_{el(2)}$ =40 min. The anode was aluminium, while the cathode was a platinum plate. Anodizing of samples was carried out in a glass bottle using a two-electrode electrochemical cell and a P-5827 M potentiostat (Gomel, Belarus) in galvanostatic mode. Prepared anodic films were cleaned in acetone and ethanol, and stored at room conditions not later than 30 days before metals immobilization (see below).

Scanning electron microscopy (SEM) and X-ray spectral analysis (EDX)

For the determination of pore diameters (D_{por}, nm) and verifying that noble metals were reduced to nanoparticles during solid phase extraction in the AAO channels, a FEI (Hillsboro, OR, USA) Quanta 400 FEG scanning electron microscope equipped with an EDAX (Mahwah, NJ, USA) Genesis V 6.04 EDX X-ray spectral analysis system was used. SEM images were taken at an accelerating voltage of 10 kV and image size of 1024x884 pixels.

Inductively coupled plasma mass spectrometry (ICP MS)

To verify the chemical stability of the produced anodic films ICP MS analysis with ELEMENT XR (Thermo Fisher Scientific, Bremen, Germany) of 5 mL water in high resolution mode (HR) before and after AAO (2 x 0.5 cm^2) immersion for 30 minutes was used with following source parameters: cool gas: 16.00 L/min; sample gas: 1.24 L/min; Faraday deflection: -217 V; plasma power: 1250 W; peri. pump speed:10 rpm; torch X-Pos. : 1.9 mm; torch Y-Pos.: 0.8 mm; torch Z-Pos.: -3.3 mm.

Micro-solid phase extraction in AAO channels

Metal stock solutions were prepared at 10 mg/mL. After dilution of the stock solutions down to concentration levels near the limit of detection (LOD), immobilization within the AAO matrix under static (24 h) and dynamic (ultrasonic bath for 30 min) conditions was carried out using several approaches:

1. Initial treatment of AAO (plate size 1×2 cm^2) by photometric reagents (NRS, dithizone, murexide, alizarin red, KI, dimethylglyoxime) followed by sorption of the targeted ions;
2. Sorption (saturation) of pre-formed photometric complex from water by AAO surface;
3. Initial sorption of ions by AAO surface followed by treatment with photometric reagents.

Photometric analysis

To qualitatively confirm presence of nanoparticles of noble metals after immobilization in AAO pores photometric analyses were carried out using a CV-2000-02 (Spectra Ltd., St. Petersburg, Russia) spectrophotometer. To transform AAO into the transparent form, the porous layer of AAO (area 1×2 cm) was separated from the aluminium barrier layer by placing the film for 30 s into 10 mM HCl. The transparent AAO films were removed from the solution, deposited on quartz plates by the Schaeffer method (horizontal lift [35]), placed into cuvettes for photometry and investigated in the wavelength range from 200 to 1100 nm (step size, 1 nm). Blank, empty AAO matrices, prepared under the same conditions, were used in these experiments.

Sorption capacities of non-transparent AAO films were evaluated using adsorption values (*a*, mol/g) [25]:

$$a = \frac{c_1 - c_2}{m} \cdot V, \quad (1)$$

where c_1 and c_2 are the initial and final concentrations of detected metal ions (mol/mL), respectively, m is the mass of the AAO plate (g) and V the volume of solution (mL).

Residual concentrations of metal ions in solution after immersion of AAO matrices were determined by conventional photometry: Pb^{2+} and Ag^{+} by reaction with dithizone, Co^{2+} with NRS, Cu^{2+} with alizarin red [36,37]. To compare sorption capacity of AAO films granular Al_2O_3 was used.

Potentiometric pH measurements

As reference system to measure the pH values of the solutions, a potentiometric sensor Multitest IPL-301 with combined electrode ESC-10603 (Cemiko Ltd., Novosibirsk, Russia) was used. The acidity of the solutions was adjusted using pH buffer mixtures.

Results and Discussion

Under the applied electrochemical conditions, regular porous structures were generated inside the utilized Al foils, with average diameters of 40-60 nm and channel lengths of up to 25 μm (Figure 1). The pores density of AAO films was 10^{10}~10^{11} pores/cm^2, with no visible external structure defects on the surface. EDX analysis of Al-films after anodization revealed the presence of Mg (due to used Al alloy) and S (sulfosalycilic electrolyte) besides Al and O lines (*Supplementary materials*, Figure S1). Subsequent ICP MS analysis showed significant migration of Al (an approx. 2.5 ppb) and Mg (approx. 300 ppt) from the films after anodization into the water (*Supplementary materials*, table S1). We interpret the increased amounts of Al and Mg in water after AAO immersion as a result of ions transport/migration through the micro-cracks occurring between barrier layer and porous matrix (*Supplementary materials*, Figure S2). Due to the combined presence of oxidized and free metallic Al within the AAO matrices, interesting properties such as reduction/oxidation abilities during metal immobilisation were expected.

Optimization of micro-solid phase extraction

As summarized in the Experimental section, three different experimental approaches for metal sorption on the AAO micro-solid extraction material were compared. The first two strategies, *i.e.*, preliminary modification of AAO by the photometric reagents followed by metal ion sorption, and sorption of the preformed photometric complex from water, unfortunately did not exhibit sufficient efficiency.

In the first approach, dithizone produced a complex with the free Al^{3+} ions that was accompanied by unstable colouring of the film surface. AAO modification with reagents containing fewer functional groups (murexide) exhibited indeed a colour change of the material, showing that a stable complex was created between target surface and photometric agent; unfortunately, after applying metal ions onto this modified surface, no visual analytical effects were seen. Similarly, immobilized NRS (3%) exhibited significant changes in the UV spectrum of the three main lines (β-, π) of the naphthoquinone forms. Moreover, the additional line at λ=527 nm along with an increased molar extinction coefficient (Figure 2, *top*) can be linked to intramolecular charge transfer initiated by the AAO matrix, readily demonstrating complex formation between Al^{3+} and functional NRS groups. NRS has a branched structure with functional groups still available after immobilization on the AAO surface. After immersion of this modified AAO matrix in $CoSO_4$ solution, a new line at λ_{436}

indicated complex formation of Co(II) and NRS (Figure 2, *bottom*) was observed. Despite the complex formation of Co(II), useful visual changes of the colour were not obtained below 0.01 mg/mL; we speculate that this was due to the partial shielding of the photometric reagent's functional groups by Al^{3+} (see above).

The second approach (immobilization of preformed photometric complexes of metal and reagent from water) did not give any visible effects, probably due to geometrical size restrictions, where the complex did not properly enter the AAO pores.

The third approach (sorption of metal ions on the AAO film, followed by treatment with photometric reagents) provided efficient immobilization of metal ions within the AAO pores regardless of whether the saturation of the AAO was performed under static or dynamic conditions (see Experimental section). The AAO films gave beneficial colour changes that were readily detected for quantification of the metal ions. Co(II) immobilized within AAO after dithizone treatment was measured down to 0.00059 mg/mL; NRS gave 0.00045 mg/mL; Pb(II) was determined at a limit of 0.00026 mg/mL using KI for visualization (Figure 3, shown for films saturated under dynamic conditions). The obtained colours were stable for at least 6 months. The limits of visual detection for Co(II), Ni(II) and Pb(II) with different photometric reagents are summarized in Table 1.

Equally no visible changes for the reported above concentrations during non-noble metals immobilisation to blank aluminium foil (before anodization) or granular Al_2O_3 were detected.

Sorption of noble metals

In the next experiment, AAO films were applied for micro-solid phase extraction of metal ions that are located right of hydrogen in the Beketov metal displacement series; *i.e.,* noble metal ions that are readily reduced to the metallic elements, for example, Ag^{+}, Cu^{2+} and Pd^{2+}. In our experiments, these ions were chemically reduced within the AAO channels, formed nanoparticular structures (Figure 4) and could not be visualized by photometric reagents as it was described above for non-noble metals.

The SEM images clearly showed visible globules of Cu-NPs and Ag-NPs of 100-1000 nm sizes on the AAO surface. UV measurements exhibited additional bands in the absorbance spectra, corresponding to metallic NPs (Table 2). The presence of multiple additional lines in the spectra for each of the tested ions probably corresponded to nanoparticular species with different diameters in the solid AAO matrix. We explain the observed effect by the presence

of free Al and Mg ions (*Supplementary materials*, table S1), resulting in chemical reduction of noble metal ions. The existence of metallic NPs on AAO was confirmed by means of SEM (Figure 4), EDX analysis (Figure 5e) and UV-spectroscopy (table 2) independently. The sorption capacity of the AAO film for noble metal ions (Cu^{2+}, Ag^{+}, Pd^{2+}) was estimated. It was found that in comparison to granular Al_2O_3 the sorption capacity (RSD ≤10 %) of AAO was approx. 13-fold larger under static, and almost 18-fold larger under dynamic conditions (Table 3). The behaviour of AAO films for noble metal ions can be explained by considering the internal matrix charge transfer between $Al^0 \leftrightarrow Al^{3+}$ from the presence of free Al. Free Al is expected to promote surface electrochemistry of AAO and stimulate Cu^{2+}, Ag^{+}, Pd^{2+} reduction to NPs by galvanic displacement (electroless deposition) [39,40]. During electroless deposition, self-assembled metallic structures are formed by galvanic displacement on the semiconductor surface. The reaction is based on *in situ* electrochemistry resulted the reduction of metal ions to NPs on the substrate in the absence of external sources of electric current or chemical reducing agents [40].

To demonstrate the observed effects occurring in the system in dynamic, we simulated the galvanic displacement of AAO by immersing the anodic films first in 10 mM HCl for 10 s and then directly in the metal ion precursor solutions (Figure 5, shown for Pd). Immersion of AAO in HCl generated characteristic etched structures, enhancing electron exchange between Al matrix and precursors solution (Figure 5b). Direct saturation of AAO with metal precursor solutions (20 mM of Pd^{2+}) leads to spontaneous metal ion reduction to NPs, with regular Pd-NPs and nanoflowers (40-100 nm) visible on the AAO (Figure 5c). Metal NPs were homogeneously distributed mostly within AAO surface without deep penetration into the porous structure (Figure 5d). Increasing of electrolysis time leads to intensive growth of larger NPs (500-800 nm), with morphology changes from nano to micro structures (Figure 5f).

Quantitative UV-detection of noble metals within AAO

Initially, several different approaches for UV-detection of noble metal ions on AAO films were utilized:

1) saturation of non-transparent AAO in noble metals solutions (accompanied by reduction of noble ions to NPs) followed by removal of Al-barrier layer and subsequent UV-detection of immobilized NPs within transparent solid matrix;
2) prior removal of Al-barrier layer followed by saturation of transparent AAO in noble metal ions solutions and photometric analyses of solid matrix;

3) immersion of non-transparent AAO in the noble metal solutions for 30 min (allowed reduction of noble metal ions to NPs) followed by conventional photometric analysis of residual ion concentration;

4) prior immobilization of photometric reagents within transparent AAO films followed by immersion in noble metal ions solutions and subsequent UV-detection of conventional photometric complex in transparent solid matrix.

Unfortunately, we have not obtained an accurate calibration for immobilized NPs directly in the AAO due to the partly dissolution of the reduced NPs during HCl treatment of the matrix (*approach 1*). Furthermore, prior removal of Al-barrier layer (*approach 2*) leading to transparent AAO films and subsequent saturation in noble metal ions solutions also didn't show an appropriate analytical effect (Figure 6a, shown for Cu^{2+}). This example demonstrated again a role of matrix surface electrochemistry (free Al from barrier layer) on the NPs formation.

Quantitative analysis of noble metal NPs was readily possible after immersion of non-transparent AAO films in the metal model solutions for 30 min (*approach 3*) followed by conventional photometric analysis (Figure 6b). Remarkably, the sorption of the noble metals by AAO exhibited a linear trend over the range from 0.3 to 3.0 mg/L.

In contrast to the described approaches above it is also highly interesting that a prior immobilization of photometric reagents within transparent AAO films followed by a further immersion in aqueous solutions of noble metals (*approach 4*) allowed a quantitative analysis of targeted ions in solid matrices (Figure 6c, shown for NRS and Cu^{2+}).

We believe that the proposed method of noble metals UV-detection within AAO matrices may have important application for NPs environment control in the future.

Conclusions

In this study, a new approach for rapid analysis of non-noble metals (Co^{2+}, Pb^{2+}, Ni^{2+}) with visual detection based on anodic aluminium oxide films was introduced. Selective electroless galvanic reduction of noble metal ions (Ag^{+}, Cu^{2+}, Pd^{2+}) within the AAO matrix allowed simultaneous UV-detection of their nanoparticles making AAO films a promising analytical tool for environmental NPs monitoring.

The next step in our study will involve investigation of sorption behavior of the non-noble metals in the presence of interfering noble ions as well as UV-quantification of NPs from the multi model solutions and waste water systems.

Acknowledgments

The authors thank Prof. Eduard Arzt (Leibniz Institute for New Materials, Saarbrücken, Germany) for continuing support of their work at INM. The authors also thank Dr. Claudia Fink-Straube (Leibniz Institute for New Materials, Saarbrücken, Germany) and Prof. Dietrich A. Volmer (Institute for Bioanalytical Chemistry, Saarbrücken, Germany) for fruitful discussion and proof-reading the paper.

References

1. K.S. Golokhvast and A.A. Shvedova, *PLoS One*, 2014, **9**, 1-11.
2. M.E. Andrus, *Russ. Metal Finish.,* 2000*,* **98**, 20-23.
3. D. Voutsa and C. Samara, *Atmos. Environ.*, 2002, **36**, 3583-3590.
4. J.E. Silva, A.P. Paiva, D. Soares, A. Labrincha and F. Castro, *J. Hazardous Mater*., 2005, **120**, 113-118.
5. G. Rossini and A. Bernardes, *J. Hazardous Mater.,* 2006*,***131**, 210-216.
6. A. Hanć*,* I. Komorowicz*,* K. Sek and D. Baralkiewicz, *J. Environ. Sci. Health. A. Tox. Hazard. Subst. Environ. Eng.*, 2009, **44**, 1441-1448.
7. R. Skorek, B. Zawisza, E. Margui, I. Queralt and R. Sitko, *Appl. Spectrosc.,* 2013*,* **67**, 204-209.
8. V.M. Ostrovskaya, A.V. Tsygankov, O.A. Prokopenko, A.K. Buryak, E.A. Reshetnyak and N.A. Nikitina. *Russ. J. Anal. Chem.*, 2008, **63**, 792-798.
9. A.V. Panteleimonov, N.A. Nikitina, E.A. Reshetnyak, L.P. Loginova, A.A. Bugaevskii and Y.V. Kholin, *Russ. Methods Objects Chem. Anal.,* 2008, **3**, 128-146.
10. S. Dong, M. Luo, G. Peng and W. Cheng, *Sens. Actuator B-Chem.*, 2008, **129**, 94-98.
11. Z. Chen and C. Lu, *Sensor Lett.,* 2005, **3**, 274-295.
12. S. Capel-Cuevas, N. Lypez-Ruiz, A. Martinez-Olmos, M.P. Cullar, M. Pegalajar, A. Palma, I. Orbe-Paub and L.F. Capitan-Vallvey, *Sensors,* 2012, **12**, 6746-6763.
13. F. Amaro*,* A.P. Turkewitz*,* A. Martín-González and J.C. Gutiérrez*, Microb. Biotechnol.*, 2011, **4**, 513-522.
14. G.H. Clever, C. Kaul and T. Carell, *Angew. Chem.*, 2007, **46**, 6226-6236.
15. I. Willner and M. Zayats, *Angew. Chem.*, 2007, **46**, 6408-6418.
16. C.X. Tang, Y. Zhao, X.W. He and X.B. Yin, *Chem. Commun.*, 2010, **46**, 9022-9024.
17. Y. Xiao, A.A. Rowe and K.W. Plaxco*, J. Am. Chem. Soc.,* 2007*,* **129**, 262-263.
18. T. Li, S. Dong and E. Wang, *J. Am. Chem. Soc.,* 2010*,* **132**, 13156-13157.
19. A. Vallée-Bélisle and K.W. Plaxco, *Curr. Opin. Struct. Biol.,* 2010, **20**, 1-9.
20. T.D. Lazzara, K.H. Lau, W. Knoll, A. Janshoff and C. Steinem, *Beilstein J. Nanotechnol.,* 2012, **3**, 475-484.
21. S. Shingubara, *J. Nanopart. Res.,* 2003, **5**, 17-30.
22. M.J. Kao, S.F. Chang, C.C. Chen and C.G. Kuo, *Eng. Technol.*, 2012, **6**, 763-766.
23. A. Mutalib Md Jani, D. Losic and N.H. Voelcker, *Prog. Mat. Sci.*, 2013, **58,** 636-704.
24. Y. Kim*,* B. Jung*,* H. Lee*,* H. Kim*,* K. Lee and H. Park*, Sensors Actuat. B-Chem.,* 2009, **141**, 441-446.

25. Y.E. Silina, B.A. Spiridonov, V.P. Gorshunova and T.A. Kuchmenko, *Russ. Anal. Control*, 2011, **15**, 324-329.
26. Y.E. Silina, T.A. Kuchmenko and D.A. Volmer, *Analyst*, 2015, **140**, 771-778.
27. A.M. Jani, D. Losic and N.H. Voelcker*, Prog. Mater. Sci.,* 2013*,* **58**, 636-704.
28. D.K. Kim, K. Kerman, H.M. Hiep, M. Saito, S. Yamamura and Y. Takamura, *Anal. Biochem*., 2008, **379**, 1-7.
29. S. Chang, H. Ko, S. Singamaneni, R. Gunawidjaja and V.V. Tsukruk, *Anal. Chem.*, 2009, **81**, 5740-5748.
30. X. Fan, I.M. White, S.I. Shopova, H. Zhu, J.D. Suter and Y. Sun, *Anal Chim Acta*, 2008, **620**, 8-26.
31. R. Nayak and D.R. Knapp, *Anal. Chem.*, 2007, **79**, 4950-4956.
32. Y.A. Barnakov, N. Kiriy, P. Black, H. Li, A.V. Yakim, L. Gu and M. Mayy, *Opt. Mater. Express*, 2011, **6**, 1061-1064.
33. J.M. Moon and A. Wei, *J. Phys. Chem. B*, 2005, **49**, 23336-23341.
34. K. Nielsch, F. Muller., A.P. Li and U. Gosele, *Adv. Mater.*, 2000, **8**, 582-586.
35. G. Roberts, *Adv. Phys.,* 1985, **34**, 475-512.
36. E.A. Reshetnyak, I.V. Ivchenko and N.A Nikitina, *Cent. Eur. J. Chem.*, 2012, **10**, 1617-1623.
37. V.M. Ostrovskaya, E.A. Reshetnyak, N.A. Nikitina, A.V. Panteleimonov and Y.V. Holin, *Russ. J. Anal. Chem*., 2004, **59**, 1101-1108 [in Russian].
38. S.K. Wang, S.H. Jeong, O.J. Lee and K.H. Lee, *Microelectron. Eng.*, 2005, **77**, 2-7.
39. H. Kawasaki, T. Yao, T. Suganuma, K. Okumura, Y. Iwaki, T. Yonezawa, T. Kikuchi and R. Arakawa, *Chem. Eur. J*., 2010, **16**, 10832-10843.
40. H.W. Tang, K.M Ng, W. Lu and C.M. Che, *Anal. Chem.,* 2009, **81**, 4720-4729.

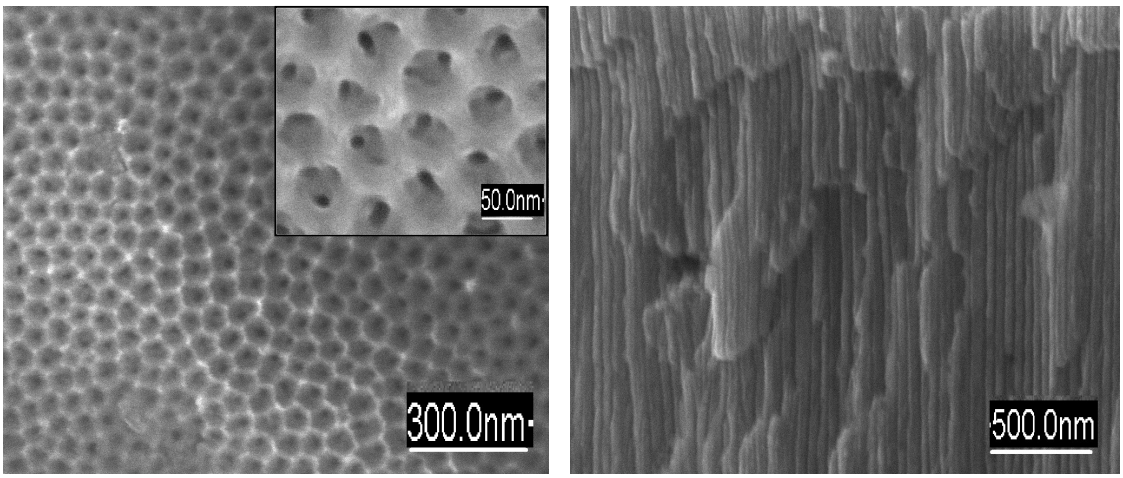

Figure 1. SEM images of AAO matrix: (*left*) surface; (*right*) cross section showing 25 μm length of porous channels.

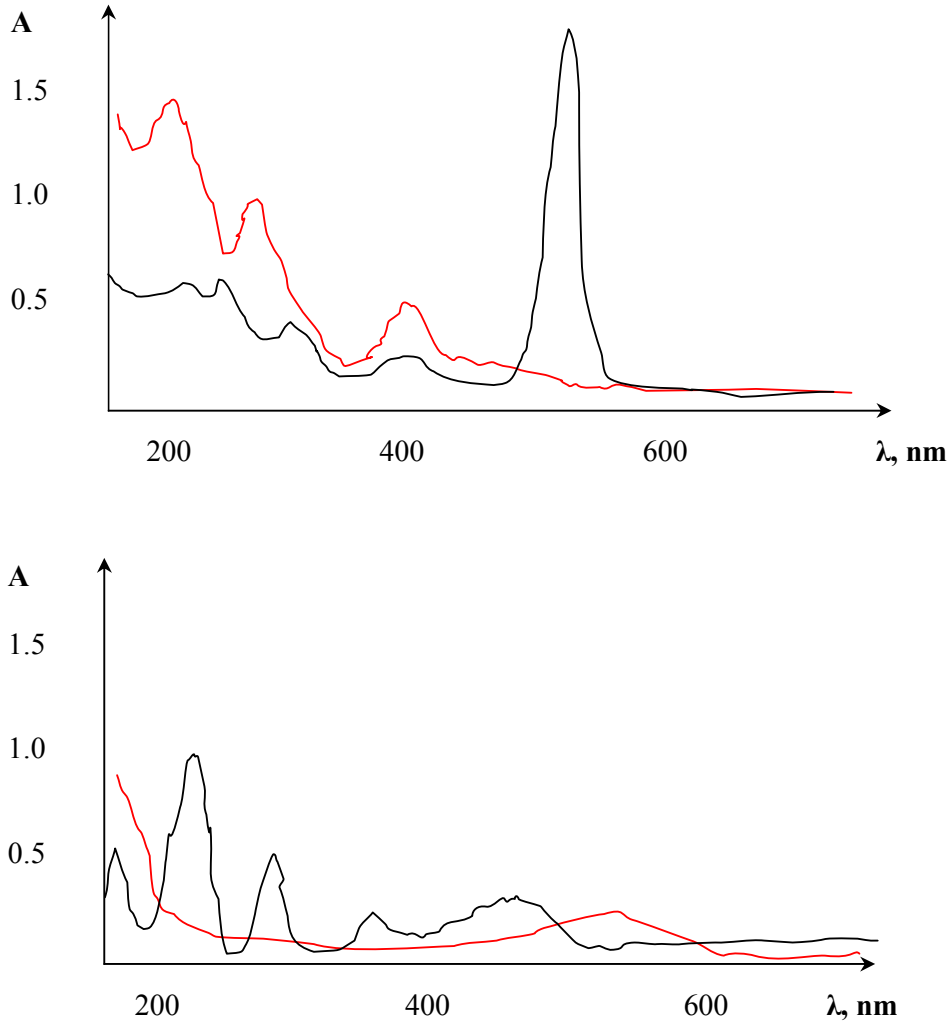

Figure 2. (*top*) Absorbance spectra of pure NRS solution (*red*); spectrum after immersion of AAO in NRS solution (*black*) (pH=4). (*bottom*) Absorbance spectra of $CoSO_4$ (0.000765 mg/mL) before AAO+NRS contact (*red*); same $CoSO_4$ (0.000765 mg/mL) after immersion of AAO+NRS (*black*), pH=4.

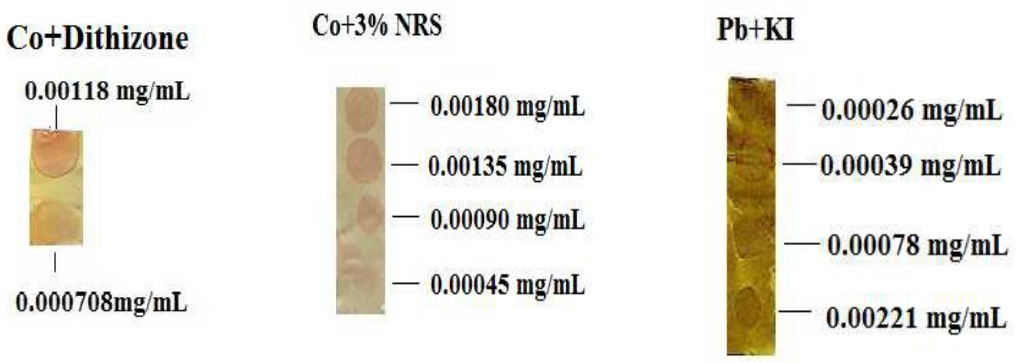

Figure 3. Images of AAO films after immobilization of non-noble ions at different concentration levels followed by photometric reagents visualization.

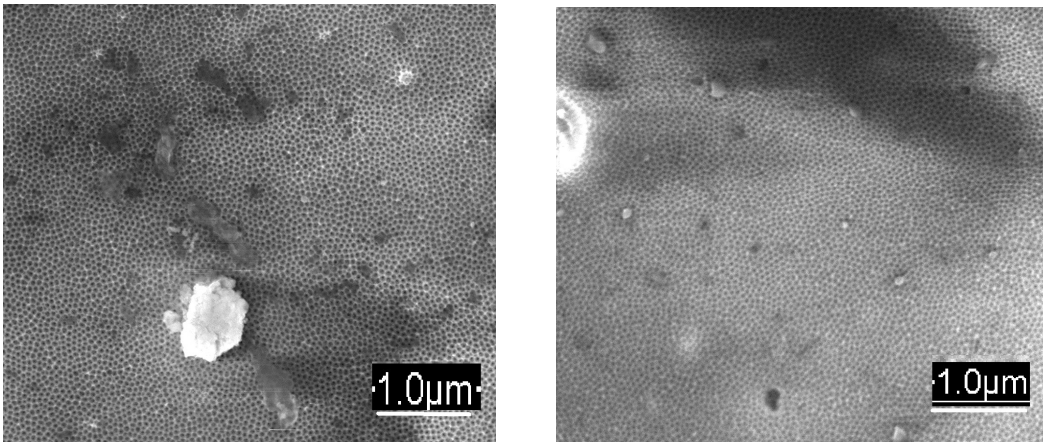

Figure 4. SEM images of AAO films after saturation (dynamic conditions) in 10 mM $CuSO_4$ (*left*) and $AgNO_3$ (*right*). The small white spots visible on both images are Cu and Ag particles after Cu^{2+} and Ag^{+} reduction.

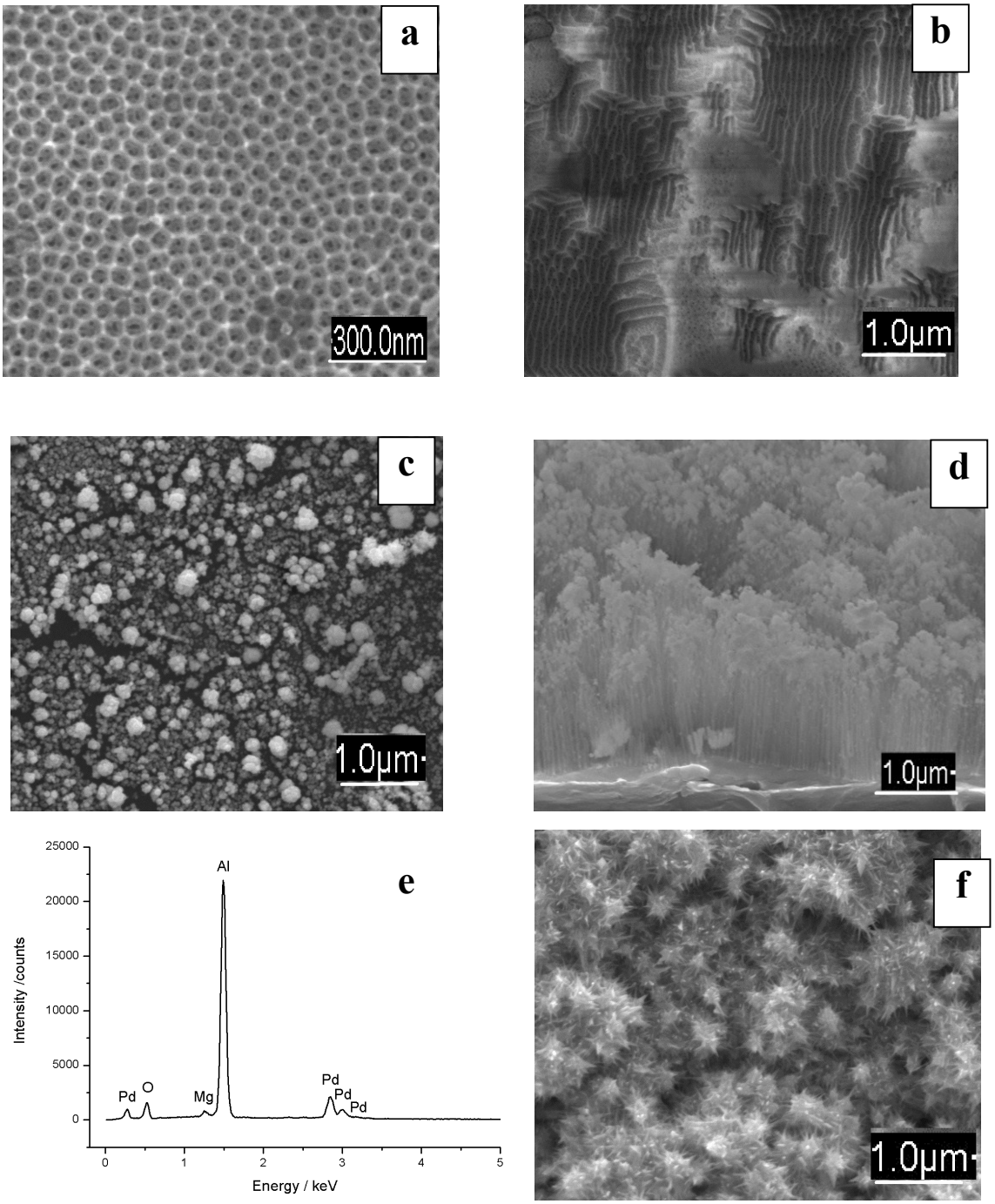

Figure 5. Illustration of Pd-NPs chemical reduction in AAO matrix during galvanic displacement: (a) pure AAO matrix; (b) etched AAO in HCI (10 s); (c) reduced Pd-NPs after immersion in precursor solution (10 s); (d) cross section of AAO matrix + Pd-NPs (10 s); (e) EDX spectra of AAO matrix after Pd-NPs reduction; (f) Pd nanoflowers (120 s duration).

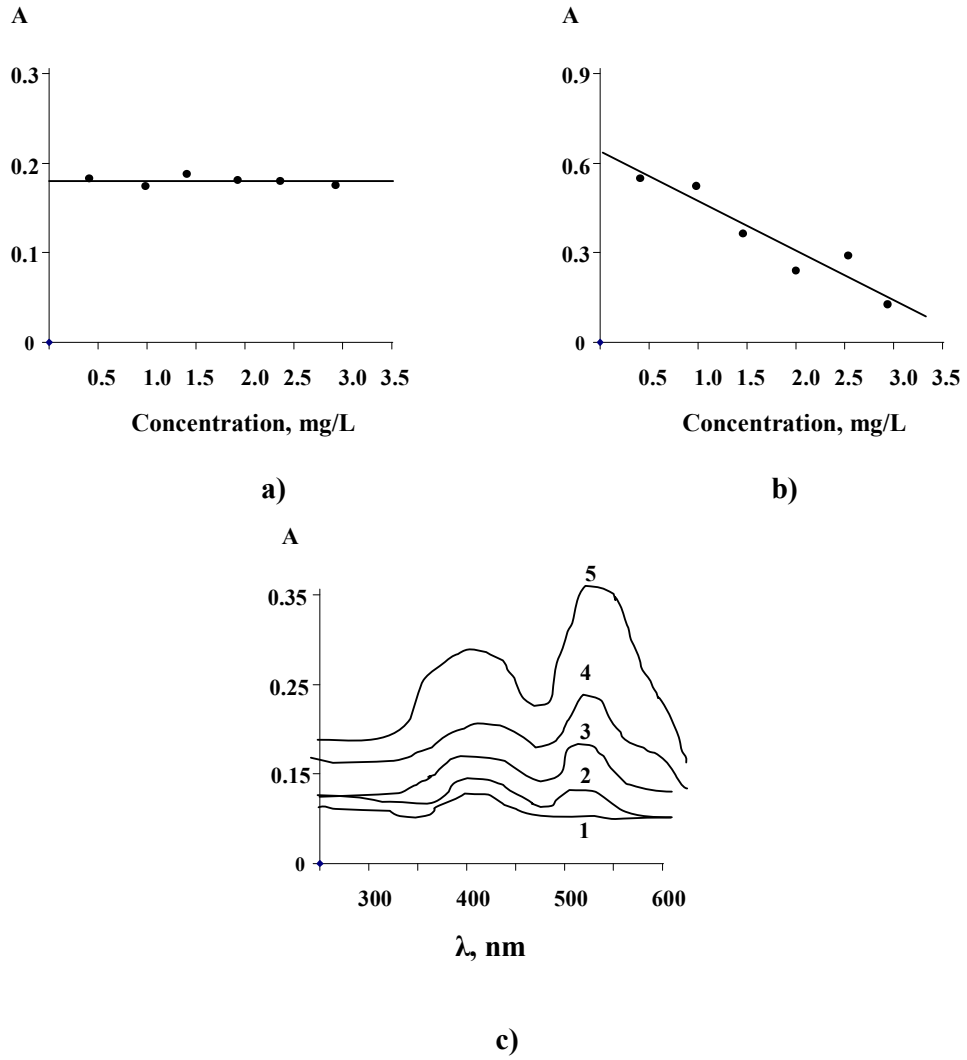

Figure 6. (*a*) Dependence of UV absorbance of transparent AAO films on Cu^{2+} concentration; (λ (Cu^0) = 387 nm). (*b*) Dependence of UV absorbance of Cu^{2+} solution (by reaction with alizarin red) on Cu^{2+} concentration; (λ (Cu^{2+}) = 515 nm); (pH = 4, immersion time of AAO with metal solution, 30 min). Note: ratio errors ($\pm\sigma$) are too small to be shown. (*c*) UV spectra of prior modified transparent AAO within NRS after emersion in Cu^{2+} solutions: 1 – 0 mg/L; 2 – 0.15 mg/L; 3 – 0.25 mg/L; 4 – 0.5 mg/L; 5 – 1.0 mg/L.

Table 1. Visible changes and obtained limits of detection on the AAO films after metal ions immobilization followed by photometric reagents treatment.

Metal ion	**Photometric reagent**	**Color**	**LOD[1] (mg/mL)**
Co^{2+}	Dithizone	yellow-red	0.00059
Co^{2+}	Nitroso-R-salts	rose	0.00045
Pb^{2+}	Dithizone	bright rose	0.00025
Pb^{2+}	Alizarin Red	violet (in ammonium buffer)	0.00030
Pb^{2+}	KI	bright yellow	0.00026
Ni^{2+}	Dimethylglyoxime	rose	0.00059

[1]LOD defined as limit concentration of element in waste water.

Table 2. Absorbance (*A*) of noble metals: solution spectra in comparison to immobilized species within solid transparent AAO films.

Ion	*A* (Solution) (λ_{max}, nm)	*A* (AAO+Me^{n+}) (λ_{max}, nm)	Note
Cu^{2+}	1.21 (515)	0.21 (355) 0.19 (387)	Additional lines at $\lambda_{355,\ 387\ nm}$ ($Cu^{2+} \rightarrow Cu^{0}$) $\lambda_{475\text{-}697,\ 943\ nm}$ ($Ag^{+} \rightarrow Ag^{0}$) $\lambda_{496,\ 690,\ 894\ nm}$ ($Pd^{2+} \rightarrow Pd^{0}$) indicate formation of NPs within the solid phase/AAO matrix
Ag^{+}	1.16 (520)	0.13 (475) 0.24 (697) 0.16 (943)	
Pd^{2+}	1.03 (530)	0.10 (496) 0.16 (690) 0.18 (894)	

Table 3. Comparison of sorption capacity (*a*, mol/g) of granulated Al_2O_3 and AAO films.

Me^{2+*}	***a***, mol/g (% RSD)**		
	Granular Al_2O_3	**AAO (static saturation)**	**AAO (dynamic saturation)**
Cu^{2+} (515 nm)	0.6 (4.5)	6.9 (3.1)	9.8 (8.6)
Ag^{+} (520 nm)	0.2 (7.8)	4.1 (5.9)	6.8 (4.2)
Pd^{2+}(530 nm)	0.7 (2.3)	8.3 (10.1)	10.1 (7.3)

*the metal ion concentration was chosen near the LOD value for these experiments;
** estimated in solutions after contact within non-transparent AAO films.